Theory of skyrmion states in liquid crystals

A. O. Leonov,[1,2,*] I. E. Dragunov,[3] U. K. Rößler,[1] and A. N. Bogdanov[1,†]

[1]*IFW Dresden, Postfach 270016, D-01171 Dresden, Germany*
[2]*Zernike Institute for Advanced Materials, University of Groningen, Groningen, 9700AB, The Netherlands*
[3]*Donetsk Institute for Physics and Technology, 340114 Donetsk, Ukraine*

Within the Oseen-Frank theory we derive numerically exact solutions for axisymmetric localized states in chiral liquid crystal layers with homeotropic anchoring. These solutions describe recently observed two-dimensional skyrmions in confinement-frustrated chiral nematics [P. J. Ackerman *et al.*, Phys. Rev. E **90**, 012505 (2014)]. We stress that these solitonic states arise due to a fundamental stabilization mechanism responsible for the formation of skyrmions in cubic helimagnets and other noncentrosymmetric condensed-matter systems.

I. INTRODUCTION

The concept of nonsingular multidimensional topological solitons (commonly referred to as *skyrmions*) plays an important role in many branches of modern physics [1]. Particularly, specific skyrmionic states can arise in condensed-matter systems with intrinsic and induced chirality [2,3]. During the past two decades regular solutions for such *chiral* skyrmions have been derived for different classes of noncentrosymmetric magnets [4–7] and liquid crystals [3,8,9]. In experiment, first indirect evidences for the existence of multidimensional chiral modulations have been reported in the precursor region of a helimagnet MnSi (see, e.g., contributions of Ref. [10] and a discussion and the bibliography in Ref. [11]). The following direct observations of chiral skyrmions in nanolayers of a cubic helimagnet $(Fe_{0.5}Co_{0.5})Si$ [12] have triggered intensive investigations of these solitonic states in different classes of noncentrosymmetric magnets (see, e.g., Refs. [13–16] and the bibliography in Ref. [17]). Chiral magnetic skyrmions are now considered as promising objects for applications in magnetic data storage technologies and in the emerging spin electronics [15,18,19].

Recently, two-dimensional axisymmetric localized strings analogous to isolated magnetic skyrmions have been optically generated in thin layers of a chiral nematic confined between substrates with perpendicular (*homeotropic*) surface anchoring [20]. During the past four decades a rich variety of 2D and 3D localized structures with different types of singularities have been observed in confined chiral liquid crystals as *cholesteric bubbles* (*spherulitic domains*) [21,22], cholesteric fingers [22,23], torons [24,25], and other specific solitonic textures [26].

Importantly that in most of nonlinear field models *static* multidimensional solitons are unstable and collapse spontaneously under the influence of internal and external perturbations (this mathematical truth is known in physicis of solitons as *Derrick-Hobart theorem* [27]). However, in condensed-matter systems lacking inversion symmetry (such as magnets, multiferroics, ferroelectrics, and chiral liquid crystals) there exist specific interactions imposed by the handedness of the underlying structure which stabilize 2D and 3D isolated states [2,4,8]. It was shown by direct calculations that this fundamental stabilization mechanism is responsible for the formation of skyrmions (nonsingular solitons) in bulk and confined chiral liquid crystals [8,9].

In this paper, we apply the nonsingular model [8,28] to investigate basic properties of two-dimensional axisymmetric skyrmions in thin layers of chiral liquid crystals (Fig. 1). By numerically solving the differential equations minimizing the Frank functional we derive the equilibrium structures of confined chiral modulations (isolated and embedded skyrmions, helicoids) as functions of the material parameters and applied electric (and/or magnetic) fields.

II. ISOLATED SKYRMIONS

Within the continuum theory the equilibrium distributions of the director $\mathbf{n}(\mathbf{r})$ in confined liquid crystals are derived by solving the Euler equations for the Frank free-energy density functional [29]

$$f(\mathbf{n}) = \frac{K_1}{2}(\text{div }\mathbf{n})^2 + \frac{K_2}{2}(\mathbf{n} \cdot \text{rot }\mathbf{n} - q_0)^2$$
$$+ \frac{K_3}{2}(\mathbf{n} \cdot \text{rot }\mathbf{n})^2 - \frac{\varepsilon_a}{2}(\mathbf{n} \cdot \mathbf{E})^2 - \frac{\chi_a}{2}(\mathbf{n} \cdot \mathbf{H})^2. \quad (1)$$

Here, K_i ($i = 1,2,3$) and q_0 are elastic constants, $\mathbf{E}$ and $\mathbf{H}$ are the vectors of applied electric and magnetic fields, and ε_a and χ_a are values of dielectric and diamagnetic anisotropies. Because dielectric and diamagnetic anisotropy energy contributions have the same functional form [Eq. (1)], they lead to the same solutions. For the sake of simplicity we consider only effects imposed by applied electric fields. We also restrict our analysis by the one constant approximation ($K_1 = K_2 = K_3 = K$).

The equilibrium states of an infinite chiral liquid crystal are characterized by two material parameters:

$$p = \frac{2\pi}{q_0}, \quad E_0 = \frac{\pi K q_0}{2}\sqrt{\frac{K}{\varepsilon_a}}, \quad (2)$$

where *helix pitch p* is the width of one complete turn ($\Delta\theta = 2\pi$) of the director $\mathbf{n}$ along the helical axis and E_0 is a value of the applied field unwinding the helix into a set of isolated kinks [29].
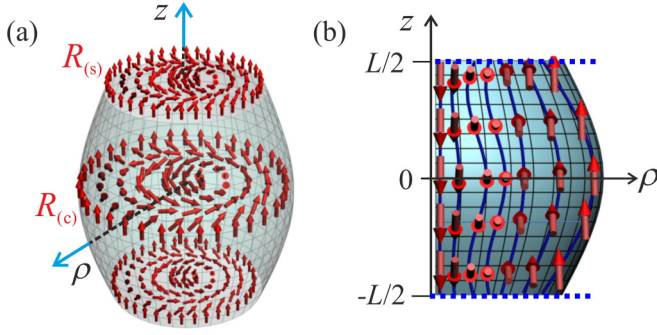
*a.leonov@rug.nl
†a.bogdanov@ifw-dresden.de

FIG. 1. (Color online) Axisymmetric skyrmion in a chiral liquid crystal layer of thickness L confined by surfaces $z = \pm L/2$ with homeotropic anchoring. The director **n** is designated by arrows to demonstrate a fixed rotation sense. (a) Due to homeotropic anchoring the cores of the surface layers (s) are smaller than in the central (c) layer. (b) Cut in the ρz half-plane shows rotation of **n** along the ρ axes for different values of z. Isoclines $\theta = \pi i/6$ ($i = 0...6$) calculated for solutions $\theta(\rho, z)$ in Fig. 2 are indicated with solid (blue) lines. Characteristic widths of the skyrmion core $R(z)$ are defined by Eq. (9).

We consider a plate infinite in x and y directions and confined by parallel planar surfaces at $z = \pm L/2$ as a model for a thin layer of a chiral nematic liquid crystal of thickness L sandwiched between two glass plates. To investigate axisymmetric localized solutions we introduce cylindrical coordinates for the spatial variable **r** and spherical coordinates for the director **n**: $\mathbf{r} = (\rho \cos \varphi, \rho \sin \varphi, z)$,

$$\mathbf{n} = (\sin \theta \cos \psi, \sin \theta \sin \psi, \cos \theta). \quad (3)$$

The total energy for isolated solutions of type $\theta = \theta(\rho, z)$, $\psi = \psi(\varphi)$ can be written as

$$F = \frac{K}{2} \int_0^{2\pi} d\varphi \int_{-L/2}^{L/2} dz \int_0^{\infty} \rho d\rho \, [w(\theta, \psi) + w_s(\theta)], \quad (4)$$

where

$$w = \left(\frac{\partial \theta}{\partial z}\right)^2 + \left(\frac{\partial \theta}{\partial \rho}\right)^2 + \frac{\sin^2 \theta}{\rho^2} \left(\frac{\partial \psi}{\partial \varphi}\right)^2 + \frac{\varepsilon_a E^2}{K} \sin^2 \theta$$

$$+ 2q_0 \left[\left(\frac{\partial \theta}{\partial \rho}\right) + \frac{\sin \theta \cos \theta}{\rho} \left(\frac{\partial \psi}{\partial \varphi}\right) \right] \sin(\psi - \phi), \quad (5)$$

the surface energy $w_s(\theta) = (K_s/K) \sin^2 \theta \, \delta(z \pm L/2)$, where $\delta(x)$ is the Dirac function. For $K_s > 0$, the energy density $w_s(\theta)$ describes a *homeotropic* anchoring.

Minimization of functional Eq. (4) yields $\psi = \varphi + \pi/2$, and the equilibrium profiles $\theta(\rho, z)$ are derived by solving the Euler equation,

$$\frac{\partial^2 \theta}{\partial z^2} + \frac{1}{\rho} \frac{\partial \theta}{\partial \rho} + \frac{\partial^2 \theta}{\partial \rho^2} - \frac{1}{\rho^2} \sin \theta \cos \theta$$

$$- \frac{2q_0}{\rho} \sin^2 \theta - \frac{\varepsilon_a E^2}{K} \sin \theta \cos \theta = 0, \quad (6)$$

with boundary conditions $\theta(0, z) = \pi$, $\theta(\infty, z) = 0$,

$$\left. \left(\frac{\partial \theta}{\partial z} + \frac{K_s}{K} \sin \theta \cos \theta \right) \right|_{z = \pm L/2} = 0. \quad (7)$$
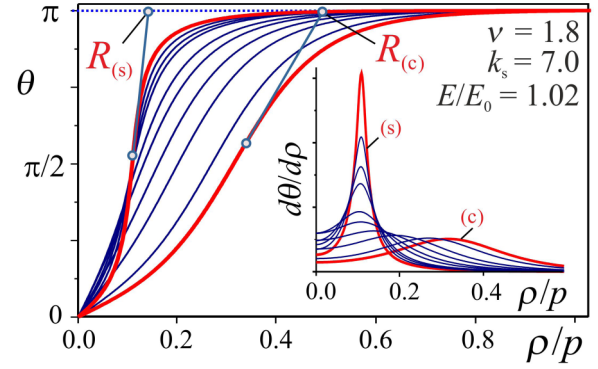

FIG. 2. (Color online) Solutions of Eqs. (6) and (7) in a layer with confinement ratio $\nu = L/p = 1.8$, surface anchoring $k_s = 7.0$, and the applied field $E = 1.02E_0$. Functions $\theta(\rho, z)$ are plotted as a set of profiles $\theta(\rho)$ for different values of z ($0 < z < L/2$). Thick (red) lines show solutions in the center (c), $\theta(\rho, 0)$ and on the surfaces (s) of the layer, $\theta(\rho, \pm L/2)$. The corresponding core sizes $R_{(c)}$, $R_{(s)}$ are derived from Eq. (9). Inset shows corresponding profiles $d\theta/d\rho(\rho)$ indicating the inflection points of $\theta(\rho)$ profiles.

The solutions $\theta(\rho, z)$ of Eqs. (6) and (7) depend on the three control parameters,

$$E/E_0, \quad k_s = K_s/(K q_0), \quad \nu = L/p, \quad (8)$$

expressed as reduced values of the applied electric field (E/E_0), the homeotropic anchoring (k_s), and the layer thickness ν known as *confinement ratio*.

The boundary value problem, Eqs. (6) and (7), has been solved by a standard finite-difference method with discretization on rectangular grids with adjustable grid spacings. As initial guess for the iterative procedure by a Seidel method with Chebishev acceleration [30], we used the known solutions of Eq. (6) for bulk chiral systems [4] as starting profiles. Solutions of Eqs. (6) and (7) $\theta(\rho, z)$ can be presented as a stack of profiles $\theta(\rho)$ parametrized by z ($-L/2 < z < L/2$) (Fig. 2). Under the influence of the homeotropic anchoring $\theta(\rho)$, curves vary along the layer thickness from wild bell-shape lines in the center of the layer ($z = 0$) to narrow profiles at the layer surface ($z = \pm L/2$). The equilibrium solutions for isolated axisymmetric skyrmions $\theta(\rho, z)$ strongly depend on the control parameters: $\nu = L/p$, E/E_0, and K_s/K_{s0} (Figs. 2 and 3). They exist only for applied fields higher than the unwinding field ($E > E_0$). Below this field, axisymmetric skyrmions are unstable with respect to elliptic distortions (similar instabilities arise in bulk chiral skyrmions [31]). Formally, the solutions for axisymmetric skyrmions with well-defined sizes exist at arbitrary high fields $E > E_0$. However, the solutions with extended cores arise only for applied fields in the close proximity of the transition field $E \gtrsim E_0$ (Figs. 2 and 3). With increasing field the core size rapidly decreases to the values comparable with the molecular length manifesting a breakdown of the continuum theory.

For a $\theta(\rho)$ line the point where the tangent at the inflection point (ρ_0, θ_0) intersects the ρ axis (Fig. 3) introduces the radius $R(z)$, which characterizes the profiles width [4,32]:

$$R = \rho_0 - \theta_0 \left(d\theta/d\rho\right)^{-1}_{\rho = \rho_0}. \quad (9)$$
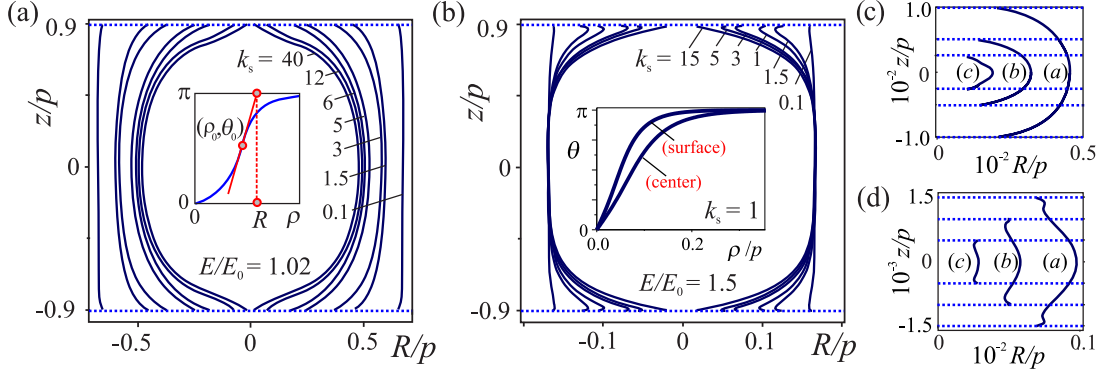
FIG. 3. (Color online) Equilibrium shapes $R(z)$ of spherulites in a layer with thickness $L = 1.8p$ and for different values of homeotropic anchoring: (a) $E = 1.02E_0$. Near the unwinding transition spherulites have extended sizes; (b) $E = 1.5E_0$. For higher fields their cores become strongly localized. Inset in panel (a) introduces the effective sizes of profiles $\theta(\rho)$ [Eq. (9)]; inset in panel (b) shows spherulites shapes in layers with thickness $L/p = 0.01(a), 0.005(b), 0.0025(c)$ $(E = 1.02E_0, K_s = 7.0K_{s0})$.

Note that a similar procedure is applied to introduce characteristic sizes for isolated domain walls and other solitonic states [31,32]. The calculated lines $R(z)$ $(-L/2 < z < L/2)$ for different values of the control parameters are plotted in Fig. 3. They have a characteristic convex shape. The homeotropic surface anchoring compresses ideally cylindrical axisymmetric solitons into convex-shaped spherulites (Figs. 3). However, a complex interplay between surface volume interactions leads to other specific effects. It was found that in an extended range of the control parameters, the functions $R(z)$ reach the minimum at a certain distance from the surface creating specific "necks" [Fig. 3(b)].

III. LINEAR ANSATZ FOR ISOLATED SPHERULITES

In a wide range of the control parameters solutions of Eqs. (6) and (7) $\theta(\rho, z)$ are composed of arrowlike profiles $\theta(\rho)$ and can be satisfactorily approached by a linear ansatz,

$$\theta(\rho, z) = \pi\rho/\xi(z), \tag{10}$$

for $\rho \leqslant \xi(z)$, and $\theta(\rho, z) = 0$ for $\rho > \xi(z)$. A trial function Eq. (10) is a specific case of a more general "scaling ansatz,"

$$\theta(\rho, z) = \theta[\rho/\xi(z)], \tag{11}$$

investigated for functional Eq. (4) in Ref. [8].

With ansatz Eq. (10) energy F Eq. (4) can be reduced to the functional $\widetilde{F}(z) = (\pi K/4) \int_{-L/2}^{L/2} [\tilde{w} + \tilde{w}_s] dz$, with

$$\tilde{w}(z) = \left(\frac{d\xi}{dz}\right)^2 + 4\pi q_0\xi + \frac{2\varepsilon_a E^2}{K}\xi^2, \tag{12}$$

and $\tilde{w}_s = (K_s/K)^2\xi^2\delta(z \pm L/2)$. Minimization of functional $\widetilde{F}(z)$ yields the equation

$$\xi(z) = \frac{4p}{\pi^2}\left(\frac{E}{E_0}\right)^{-2}\left[1 - \frac{1}{\Omega(\nu, k_s)}\cosh\left(\frac{\alpha z}{p}\right)\right], \tag{13}$$

describing a *catenary* curve. Here $\alpha = \pi(E/E_0)$ and

$$\Omega(\nu, k_s) = \cosh\left(\frac{\alpha\nu}{2}\right) + \frac{\pi^2 k_s}{2}\sinh\left(\frac{\alpha\nu}{2}\right). \tag{14}$$

The control parameters (ν, k_s, E/E_0) Eq. (8) determine curvature and other parameters of Eq. (13) (for details see

Ref. [8]). Comparison with solutions of Eqs. (6) and (7) shows that calculations with linear ansatz Eq. (10) reaches a satisfactory quantitative accuracy only for weak anchoring ($k_s \ll 1$). Nevertheless analytical results for model Eq. (12) offer an important insight into physics of confined chiral skyrmions.

The equilibrium sizes of spherulites are formed as a result of a competition between the terms linear and quadratic with respect to ξ in functional Eq. (12). The former ($\propto q_0$) is stemmed from the *chiral* interactions imposed by the handedness of the system and which are represented in Frank functional with energy contributions linear with respect to the first spatial derivatives:

$$w_q(\mathbf{n}) = 2K_2q_0\mathbf{n} \cdot \text{rot}\mathbf{n}. \tag{15}$$

The latter includes internal interactions independent on spatial derivatives of $\mathbf{n}$ (as the dielectric anisotropy energy $\propto E^2$ in functional Eq. (5). Finally, the first term in Eq. (12) determines a variation of the equilibrium core size $\xi(z)$ along the layer thickness imposed by the surface anchoring. Note, functional Eq. (12) does not include the energy contributions quadratic in the spatial derivatives [*spray-twist-band* elastic energy contributions in Eq. (1)]. Solutions, Eq. (13), for functional Eq. (12) display in a simple form the fundamental features of the chiral skyrmion energetics and elucidate a crucial role of the chiral energy $w_q(\mathbf{n})$ in their formation. Energy contribution $w_q(\mathbf{n})$ arises in chiral liquid crystals [29] and cubic noncentrosymmetric magnets [2,33] and are composed of antisymmetric differential forms linear with respect to spatial derivatives of the order parameter $\mathbf{l}$ (so called Lifshitz invariants) [33]:

$$\Lambda_{ij}^{(k)} = l_i\frac{\partial l_j}{\partial x_k} - l_j\frac{\partial l_i}{\partial x_k}. \tag{16}$$

Energy functionals of noncentrosymmetric condensed-matter systems contain chiral energy contributions $w_{\text{chiral}}(\mathbf{l})$ constructed of the combinations of differential forms, Eq. (16), complied with their symmetry [2,33]. Particularly for isotropic and cubic systems $w_{\text{chiral}}(\mathbf{l})$ reduced to $w_q(\mathbf{l}) = \Lambda_{yx}^{(z)} + \Lambda_{xz}^{(y)} + \Lambda_{zy}^{(z)} = \mathbf{l} \cdot \text{rot}\mathbf{l}$, describing chiral interactions in liquid crystals and noncentrosymmetric cubic magnets and ferroelectrics,

Eq. (15) [5,29,33,34]. Energy contributions composed of differential forms of Eq. (16) provide a specific stabilization mechanism for two- and three-dimensional localized states [2]. Importantly, classical skyrmions intensively investigated in nonlinear physics are stabilized by higher-order spatial derivatives of the order parameter (commonly referred to as *Skyrme mechanism* [1]). Because in condensed-matter physics there are no physical interactions described by higher-order spatial derivatives (se, e.g., Ref. [7] in Ref. [6]), noncentrosymmetric condensed-matter systems (including chiral liquid crystals, multiferroics, and magnetic systems with intrinsic and induced chirality) are of special importance as a particular class of materials where mesoscopic skyrmions can be created and manipulated. This also attaches special importance to the solutions of Eqs. (6) and (7) as basic elements providing the stability of axisymmetric skyrmions and other solitonic states observed in chiral liquid crystals layers [20,22].

IV. CONFINED SKYRMION LATTICES AND HELICOIDS

In unconfined chiral liquid crystals solutions for axisymmetric skyrmions are homogeneous along their axes [solutions of type $\theta(\rho)$, $\psi = \pi/2 + \varphi$] [3]. For $E < E_0$, Eq. (2), the one-dimensional modulated states (*helices*) correspond to the global minimum of the system [29]. Below critical field E_0 chiral skyrmions condense into *metastable* lattices [3]. Near the critical field E_0 skyrmion lattices transform into honeycomb nets of thin 180° walls. Helices in this region consist of broad stripes (with $\theta \approx 0$) separated with thin 180° walls. The equilibrium periods of the helices and skyrmion lattices tend to infinity as $E \to E_0$, and both modulated phases transform into the homogeneous state in the same critical point (Fig. 10 in Ref. [3]). Contrary to bulk systems, in thin layers chiral modulations become inhomogeneous through the layer thickness. Here we consider main effects imposed by the homeotropic anchoring on helicoids and skyrmion lattices with propagation directions in the layer plane. Within a circular-cell approximation (see, e.g., Ref. [3]), the equilibrium parameters of a skyrmion lattice are derived by solving Eq. (6) with the boundary conditions $\theta(0,z) = 0$, $\theta(a,z) = \pi$, Eq. (7), for different values of the cell size a and minimization of the skyrmion lattice energy density with respect to a. Similarly, the equilibrium states of a 2D helicoid propagating along the y axis in the layer plane, $\mathbf{n} = [\sin\theta(y,z), 0, \cos\theta(y,z)]$ are derived by solving equation

$$\frac{\partial^2\theta}{\partial z^2} + \frac{\partial^2\theta}{\partial y^2} - \frac{\pi^2}{16}\left(\frac{E}{E_0}\right)^2 \sin\theta\cos\theta = 0, \quad (17)$$

with the boundary conditions $\theta(0,z) = 0$, $\theta(b,z) = 2\pi$, Eq. (7) and optimization of the helix energy density with respect to pitch b. Typical solutions for Eq. (17) are presented in Fig. 4(a) as $\theta(z)$ profiles in the equidistant xz planes for a number of fixed values of y (indicated with thin black lines). Similarly to confined skyrmions, helix profiles $\theta(y,z)$ have a convex shape in the xz planes. The distribution of the energy density in the helicoid along the propagation direction y is plotted in Fig. 4(a) for the surfaces $z = \pm L/2$ (dashed blue line) and in the center of the layer $z = 0$ (solid red line). The largest loss of the rotational energy occurs for the planes with $\theta = \pi/2$. Similar energy densities $w(\rho)$ for the isolated
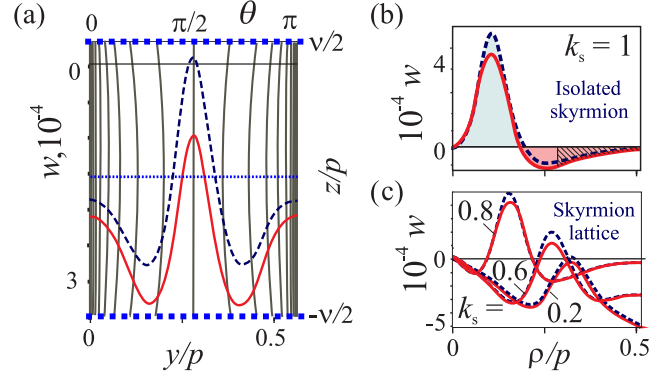
FIG. 4. (Color online) Typical solutions for confined helicoids (a). Top and right axes show profiles $\theta(z)$ in equidistant planes xz. Lower and left axes show energies densities: dashed (blue) lines correspond to surface layers ($z = \pm L/2$) and the solid (red) line is for the center of the layer ($z = 0$). Corresponding energy densities for an isolated sherulite and a skyrmion lattice are plotted in panels (b) and (c).

spherulite and the skyrmion lattice cell are plotted in Figs. 4(b) and 4(c). The results of the calculations for confined helices and skyrmion lattices in a layer with $\nu = 1.8$ are presented in the phase diagram in reduced variables E/E_0 and k_s (Fig. 5). The confined helicoid is the global minimum of the system in the area below critical line $E_h(k_s)$. A sufficiently strong homeotropic anchoring suppresses helical modulations and above $E_h(k_s)$ line the homogeneous phase with $\theta = 0$ has the lowest energy. In this "saturate" phase isolated spherulite can exist as metastable states. The skyrmion lattices can exist as metastable states below critical line $E_{sk}(k_s)$ and transform into the homogeneous state at this critical line. Below $E_h(k_s)$ line isolates spherulites are eliptically unstable (cf. Ref. [31]) and strip out into helicoids or into specific textures consisting of elongated 2D solitons (so called cholesteric fingers). Experimental investigations of these modulated states are reviewed in Ref. [22].
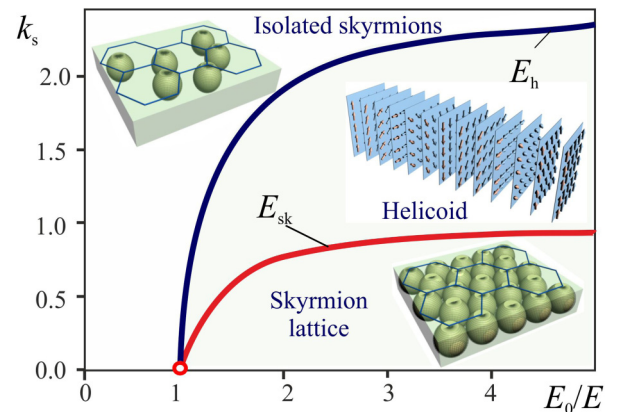
FIG. 5. (Color online) The phase diagram of the equilibrium states in reduced values of applied field (E/E_0) and homeotropic anchoring (k_s), Eq. (8), indicate the existence areas of the helicoid and the skyrmion lattice in a layer with the confinement ratio $\nu = 1.8$.

V. COMPARISON WITH MAGNETIC CHIRAL SKYRMIONS

Chiral magnetic skyrmions have been observed in nanolayers of cubic helimagnets [12–14] and monolayers of ferromagnetic metals with induced chiral interactions [15]. It was established that surface- and interface-induced uniaxial anisotropy plays a crucial role to stabilize skyrmions in these systems [14,15,17]. Theoretically, chiral modulations in nanolayers of chiral ferromagnets are described by the energy density functional [6,14,17,33],

$$f_m = A(\text{grad}\,\mathbf{m})^2 + D\mathbf{m} \cdot \text{rot}\,\mathbf{m} - \mathbf{H} \cdot \mathbf{M} - K_u(\mathbf{m} \cdot \mathbf{a})^2, \tag{18}$$

which includes the exchange energy with coefficient A, the Dzyaloshinskii-Moriya coupling (D), the interaction with the applied magnetic field $\mathbf{M}$ (Zeeman energy), and induced uniaxial anisotropy (K_u). $\mathbf{m} = \mathbf{M}/|\mathbf{M}|$ is the unity vector along the magnetization $\mathbf{M}$, and $\mathbf{a}$ is the unity vector along the uniaxial anisotropy axis (along z axis in this paper). For chiral liquid crystals in applied electric fields the Frank free-energy density functional in the one-constant approximation can be reduced to the following expression:

$$f_v = \frac{K}{2}(\text{grad}\,\mathbf{n})^2 + Kq_0\mathbf{n} \cdot \text{rot}\,\mathbf{n} - \frac{\varepsilon_a}{2}(\mathbf{n} \cdot \mathbf{E})^2. \tag{19}$$

We use here equation $(\text{grad}\,\mathbf{n})^2 = (\text{div}\,\mathbf{n})^2 + (\mathbf{n} \cdot \text{rot}\,\mathbf{n})^2 + (\mathbf{n} \times \text{rot}\,\mathbf{n})^2 + <\text{surface terms}>$ holding for any unity vector $\mathbf{n}$ (for details see, e.g., Ref. [32]). At zero field the energy density of a cubic helimagnet, Eq. (18), has the same functional form with that of a chiral liquid crystal, Eq. (19). Thus, the solutions for skyrmions derived within model Eq. (18) [4,6,17] at zero field describe skyrmions in bulk chiral liquid crystals at applied electric (magnetic) fields. Also, the energy functional for noncentrosymmetric antiferromagnets (Eq. (8) in Ref. [35]) has a similar structure with functional Eq. (19). Physical relations between magnetic and liquid crystal skyrmionic states have been discussed in Ref. [3]. It is known that surface- and interface-induced enhanced perpendicular uniaxial anisotropy arising in nanolayers of magnetic metals imposes a number of reorientation effects [36], which are similar to those induced by surface anchoring in liquid crystals [29]. In existing epitaxial layers of cubic helimagnets synthesized on Si(111) substrates, a uniaxial magnetic anisotropy is imposed by strains arising due to the lattice mismatch between the magnetic layer and the substrate [37]. In these nanolayers, the induced anisotropy has a volume-like character [see Eq. (18)]. However, in nanolayers of noncentrosymmetric magnets with induced anisotropy localized on their surfaces, chiral skyrmions and helicoids are described by equations similar to those considered in this paper [Eqs. (6), (7), and (17)]. Finally, we mention that surface twisted modulations recently discovered in nanolayers of cubic helimagnets [38] are expected to occur in confined chiral liquid crystals.

VI. CONCLUSIONS

We present numerically exact solutions for isolated and embedded axisymmetric skyrmions in a thin layer of a chiral liquid crystal with homeotropic anchoring. In this paper, we restrict our theory to the simplified model, Eq. (1), including only basic interactions *essential* to stabilize skyrmionic states [3,16], and demonstrate a fundamental role of axisymmetric strings [Eqs. (6) and (7)] in the formation of two-dimensional solitonic states in thin layers of chiral liquid crystals. The interplay between the elastic stiffness, chiral twists, and perpendicular surface leads to the formation of 2D skyrmions with a characteristic "barrel" (spherulite) shape (Fig. 1). The basic equations for confined axisymmetric skyrmions [Eqs. (6) and (7)] and other chiral modulations depend on three material parameters, Eq. (8). A few representative samples in Figs. 2, 3, and 4 illustrate the basic features of confined chiral modulations.

Multidimensional modulated textures observed in confined chiral liquid crystals have more complex structures including different types of point defects and dislocations [20–26]. Detailed analysis of these patterns requires the constructions of the full phase space of the control parameters ($E/E_0, k_s, \nu$) and calculations of 2D and 3D chiral solitons with point and linear singularities.

ACKNOWLEDGMENTS

[1] *The Multifaceted Skyrmion*, edited by G. E. Brown and M. Rho (World Scientific, Singapore, 2010).

[2] A. Bogdanov, Pis'ma Zh. Eksp. Teor. Fiz. **62**, 231 (1995) [JETP Lett. **86**, 247 (1995)]; A. N. Bogdanov, D. A. Yablonsky, Zh. Eksp. Teor. Fiz. **95**, 178 (1989) [JETP **68**, 101 (1989)].

[3] A. N. Bogdanov and A. A. Shestakov, Zh. Eksp. Teor. Fiz. **113**, 1675 (1998) [JETP **86**, 911 (1998)]; A. N. Bogdanov, U. K. Rößler, and A. A. Shestakov, Phys. Rev. E **67**, 016602 (2003).

[4] A. Bogdanov and A. Hubert, J. Magn. Magn. Mater. **138**, 255 (1994); **195**, 182 (1999).

[5] U. K. Rößler, A. N. Bogdanov, C. Pfleiderer, Nature **442**, 797 (2006).

[6] A. B. Butenko, A. A. Leonov, U. K. Rößler, and A. N. Bogdanov, Phys. Rev. B **82**, 052403 (2010).

[7] A. B. Borisov and F. N. Rybakov, Low Temp. Phys. **36**, 766 (2010).

[8] A. N. Bogdanov, JETP Lett. **71**, 85 (2000).

[9] J. Fukuda and S. Zumer, Nature Comm. **2**, 246 (2011).

[10] S. Muhlbauer *et al.*, Science **323**, 915 (2009); C. Pappas, E. Lelièvre-Berna, P. Falus, P. M. Bentley, E. Moskvin, S. Grigoriev, P. Fouquet, and B. Farago, Phys. Rev. Lett. **102**, 197202 (2009).

[11] H. Wilhelm *et al.*, J. Phys.: Condens. Matter **24**, 294204 (2012).

[12] X. Z. Yu *et al.*, Nature (London) **465**, 901 (2010).

[13] S. Seki *et al.*, Science **336**, 198 (2012).

[14] S. X. Huang and C. L. Chien, Phys. Rev. Lett. **108**, 267201 (2012); M. N. Wilson, E. A. Karhu, A. S. Quigley, U. K. Rößler, A. B. Butenko, A. N. Bogdanov, M. D. Robertson, and T. L. Monchesky, Phys. Rev. B **86**, 144420 (2012).

[15] S. Heinze *et al.*, Nature Phys. **7**, 713 (2011); N. Romming *et al.*, Science **341**, 636 (2013).

[16] U. K. Rößler, A. A. Leonov, A. N. Bogdanov, J. Phys. Conf. Ser. **303**, 012105 (2011).

[17] M. N. Wilson, A. B. Butenko, A. N. Bogdanov, and T. L. Monchesky, Phys. Rev. B **89**, 094411 (2014).

[18] N. S. Kiselev *et al.*, J. Phys. D **44**, 392001 (2011).

[19] A. Fert, V. Cros, and J. Sampaio, Nat. Nano **8**, 152 (2013).

[20] P. J. Ackerman, R. P. Trivedi, B. Senyuk, J. van de Lagemaat, and I. I. Smalyukh, Phys. Rev. E **90**, 012505 (2014).

[21] M. Kawachi, O. Kogure, and Y. Kato, Japan. J. Appl. Phys. **13**, 1457 (1974); W. E. L. Haas and J. E. Adams, Appl. Phys. Lett. **25**, 263 (1974).

[22] P. Oswald and P. Pieranski, *Nematic and Cholesteric Liquid Crystals* (Taylor&Francis Group, London, 2005).

[23] I. I. Smalyukh, B. I. Senyuk, P. Palffy-Muhoray, O. D. Lavrentovich, H. Huang, E. C. Gartland, Jr., V. H. Bodnar, T. Kosa, and B. Taheri, Phys. Rev. E **72**, 061707 (2005).

[24] I. I. Smalyukh *et al.*, Nature Mater. **9**, 139 (2010); P. J. Ackerman, Z. Qi, and I. I. Smalyukh, Phys. Rev. E **86**, 021703 (2012).

[25] B. G. Chen, P. J. Ackerman, G. P. Alexander, R. D. Kamien, and I. I. Smalyukh, Phys. Rev. Lett. **110**, 237801 (2013).

[26] M. B. Pandey, T. Porenta, J. Brewer, A. Burkart, S. Čopar, S. Žumer, and I. I. Smalyukh, Phys. Rev. E **89**, 060502 (2014).

[27] G. H. Derrick, J. Math. Phys. **5**, 1252 (1964).

[28] T. Akahane and T. Tako, Jpn. J. Appl. Phys. **15**, 1559 (1976).

[29] P. G. De Gennes, J. Prost, *The Physics of Liquid Crystals* (Oxford University Press, Oxford, 1993); M. Kleman, O. D. Lavrentovich, *Soft Matter Physics: An Introduction* (Springer-Verlag, New York, 2003).

[30] W. H. Press, S. A. Teukolsky, W. T. Vetterling, and B. P. Flannery, *Numerical Recipes: The Art of Scientific Computing* (Cambridge University Press, Cambridge, 2007).

[31] A. Bogdanov and A. Hubert, Phys. Stat. Sol. (b) **186**, 527 (1994).

[32] A. Hubert and R. Schäfer, *Magnetic Domains* (Springer, Berlin, 1998).

[33] I. E. Dzyaloshinskii, Sov. Phys. JETP **20**, 665 (1964); P. Bak and M. H. Jensen, J. Phys. C: Solid State Phys. **13**, L881 (1980).

[34] D. C. Wright and N. D. Mermin, Rev. Mod. Phys. **61**, 385 (1989).

[35] A. N. Bogdanov, U. K. Rößler, M. Wolf, and K. H. Müller, Phys. Rev. B **66**, 214410 (2002).

[36] A. Thiaville and A. Fert, J. Magn. Magn. Mater. **113**, 161 (1992); A. N. Bogdanov, U. K. Rößler, and K. H. Müller, *ibid.* **238**, 155 (2002).

[37] E. A. Karhu, S. Kahwaji, T. L. Monchesky, C. Parsons, M. D. Robertson, and C. Maunders, Phys. Rev. B **82**, 184417 (2010); E. A. Karhu, U. K. Rößler, A. N. Bogdanov, S. Kahwaji, B. J. Kirby, H. Fritzsche, M. D. Robertson, C. F. Majkrzak, and T. L. Monchesky, *ibid.* **85**, 094429 (2012).

[38] S. A. Meynell, M. N. Wilson, H. Fritzsche, A. N. Bogdanov, and T. L. Monchesky, Phys. Rev. B **90**, 014406 (2014).